Applied Catalysis B: Environmental 200 (2017) 1–9

Contents lists available at ScienceDirect

Applied Catalysis B: Environmental

journal homepage: www.elsevier.com/locate/apcatb

Passivated co-doping approach to bandgap narrowing of titanium dioxide with enhanced photocatalytic activity

Sutassana Na Phattalung[a,*], Sukit Limpijumnong[b,c,d], Jaejun Yu[e]

[a] Department of Basic Science and Physical Education, Faculty of Science at Si Racha, Kasetsart University, Si Racha Campus, Chonburi 20230, Thailand
[b] School of Physics and NANOTEC-SUT Center of Excellence on Advanced Functional Nanomaterials, Suranaree University of Techonology, Nakhon Ratchasima 30000, Thailand
[c] Thailand Center of Excellence in Physics (ThEP Center), Commission on Higher Education, Bangkok 10400, Thailand
[d] Synchrotron Light Research Institute, Nakhon Ratchasima 30000, Thailand
[e] Center for Theoretical Physics, Department of Physics and Astronomy, Seoul National University, Seoul 08826, Republic of Korea

ARTICLE INFO

Article history:
Received 25 November 2015
Received in revised form 25 March 2016
Accepted 22 June 2016
Available online 23 June 2016

Keywords:
Co-dopants in TiO_2
Band gap narrowing
Photocatalytic activity

ABSTRACT

Aiming for the enhanced photocatalytic activity of titanium dioxide (TiO_2), we probe various co-doping pairs of impurity atoms in TiO_2 in search of the right co-dopants which can reduce the bandgap without creating recombination centers. To confirm the band edges and the relative positions of impurity levels, we perform first-principles density-functional-theory calculations within the local density approximation as well as the hybrid functional approach. From the analysis of the bandgaps of doped-TiO_2 and the defect levels, we propose that the vanadium-nitrogen (V-N) pair is a suitable passivated co-dopant in TiO_2. By doping TiO_2 with the V-N pair, the bandgap of TiO_2 is reduced; enhancing the visible light absorption. The calculated band edges after doping also matches the redox potentials of hydroxyl radical ($^{\bullet}OH$) and superoxide anion ($O_2^{\bullet -}$); enhancing the photocatalytic activity for the degradation of organic pollutants and acting as antibacterial agents as well.

1. Introduction

Titanium dioxide (TiO_2) is an efficient photocatalyst used in various applications such as hydrogen production through water splitting, the degradation of organic pollutants and antibacterial agents. Many researchers have directed their attentions toward the use of TiO_2 as a photocatalyst using solar energy. Although TiO_2 has high oxidizing power and high chemical stability, making it suitable as a photocatalyst, its major drawback is its large band gap of 3.23 eV. The large band gap limits its photon absorption to only a small portion of the solar spectrum. To utilize a wider range of the sunlight, the band gap of TiO_2 needs to be narrowed. It is generally preferred that the absolute positions of the band edges are engineered to locate at the levels suitable for water splitting in order to acquire hydrogen as a clean and renewable energy source [1–4]. In addition, the reduced band-gap TiO_2 can be adapted as an antibacterial agent [5] and an agent for the degradation of organic pollutants [6].

Doping by anions has been reported to be a way to reduce the band gap of TiO_2 [1–4]. However, anion-doping generally causes a lower photocatalytic activity [7] due to the reduction of the redox potential of photoelectrons or photoholes. While the bandgap reduction can enhance light absorption efficiency in the visible range, it also causes either less negative electron potential or less positive hole potential [8]. As a result, the overall photocatalytic activity under visible light is reduced compared to that under UV light. Indeed it is one of the most challenging subjects in current photocatalytic research to develop a TiO_2 photocatalyst that can maintain a strong redox potential and, at the same time, utilize visible-light (vis) photons.

To remedy the reduction of the redox potential, it is necessary to carefully choose proper dopants that give the positions of donor and acceptor levels matching the redox potentials of the adsorbate. There has been a large number of research works focusing on the doping of TiO_2 by various dopants: including anions (B [9], C [10], N [11–16], chalcogen [17], and halogen atoms [11,18–23]) as well as cations [11,18–29]. Most of initial attempts were focused only on narrowing the band gap of TiO_2. In principle, mono-doping can reduce the band gap, but usually it introduces partially occupied defect levels that acts as a carrier recombination center. Consequently the mono-doping ends up reducing band gap and at

* Corresponding author.
E-mail addresses: sutassana@gmail.com (S. Na Phattalung), jyu@snu.ac.kr (J. Yu).

http://dx.doi.org/10.1016/j.apcatb.2016.06.054
0926-3373/

the same time unintentionally reduces the photocatalytic activity [22,30,31].

Obviously doping TiO_2 with a single dopant is not sufficient to simultaneously obtain the desired band gap and maintaining a proper redox potential, especially, for photocatalyst applications. Since the charge state and defect energy levels of an impurity are often affected by the presence of another impurity atom, the use of co-dopants can be quite effective for the control of band gap as well as the position of impurity levels. To find the right combination of co-dopants for a given photocatalyst application, we propose a passivated co-doping approach that can reduce the band gap without creating any recombination center. The main idea is that the defect levels, when successfully passivated, do not act as carrier-recombination centers [3,32,33]. Therefore, the fully passivated co-doping can suppress the carrier recombination center problems in TiO_2 [3].

In this work, we investigated various co-doping pairs of impurity atoms in TiO_2. We propose the vanadium and nitrogen (V-N) pair to be a suitable cation-anion co-dopant in TiO_2 for an efficient antibacterial agent application. To understand the electronic properties of TiO_2 doping with potential cations and anions candidates, we carried out first-principles density-functional-theory calculations. The electronic structure and projected density-of-states (pDOS) were obtained. Among various possible mono-doping and co-doping configurations, we analyzed the shift of band edges and the positions of impurity levels to identify dopants with the band gap optimized for the visible light absorption without the recombination centers. From the results, we found that the V-N co-doping pair satisfies the reduced band gap and the passivation condition as well. The TiO_2 doped with V-N co-dopant has a reduced band gap that matches the redox potential for of hydroxyl radical ($^{\bullet}OH$) and superoxide anion ($O_2^{\bullet -}$). Therefore, it is expected that TiO_2 doped with V-N pair should have enhanced photocatalytic activity under the visible range of the solar spectrum for the degradation of organic pollutants and antibacterial agent applications.

2. Calculational methods

To investigate the electronic structure, impurity levels, and formation energies of TiO_2 with impurity atoms, we carried out density functional theory (DFT) calculations under the local density approximation (LDA) and projector augmented wave (PAW) [34], as implemented in the VASP codes [35]. The calculated lattice parameters of bulk anatase TiO_2 are $a = 3.764$ Å, $c/a = 2.488$, and $u = 0.208$, which are in good agreement with the experimental values of $a = 3.785$ Å, $c/a = 2.513$, and $u = 0.208$ [36] and other calculations [37–39]. Our calculated TiO_2 band gap of 2.48 eV is in agreement with the calculations by other groups [40,41], but smaller than the experimental band gap of 3.23 eV [42] due to the well-known DFT problems. This LDA band gap underestimation poses an uncertainty in the calculated levels associated with impurities. In order to obtain more realistic energy levels associated with selected promising impurities, namely vanadium, nitrogen, and vanadium-nitrogen co-doped systems, were recalculated using the Heyd-Scuseria-Ernzerhof hybrid functional (HSE06) [43–45] which is much more computational demanding. The TiO_2 band gap calculated with HSE06 is 3.30 eV, which is in good agreement with the experimental band gap. Therefore, the energy levels obtained by HSE06 calculations can be directly compared with experiments without band gap corrections and therefore believed to be more reliable.

To study defects, a supercell approach was used [46–48]. In the calculations, a plane-wave basis set with the cutoff energy of 400 eV was used and all atoms were allowed to relax until the Hellmann-Feynman forces become less than 0.05 eV/Å. Our preliminary calculations used a supercell containing 48 atoms, which is a $2 \times 2 \times 2$ repetition of the primitive anatase unit cell. To ensure the cell size convergence, all calculations were repeated with a larger supercell containing 96 atoms, which is a $4 \times 2 \times 2$ repetition of the primitive anatase unit cell. It is found that the defect formation energies calculated using the 48-atom cells are in agreement with the corresponding ones, calculated using the 96-atom cells, to within 0.4 eV. For the Brillouin zone integrations, a shifted $2 \times 2 \times 2$ Monkhorst-Pack [49] special k-point mesh was used (for both supercell sizes). All numerical results presented in this work are based on the 96-atom cell calculations except for the HSE06 calculations where only the 48-atom cell is used due to a much more computational demand of the method.

The formation energy of an impurity D in charge state q is defined [46,47], as

$$E^f\left[D^q\right] = E_{\text{tot}}\left[D^q\right] - E_{\text{tot}}\left[\text{TiO}_2, \text{bulk}\right] + \sum_x \Delta n_x \mu_x + q\left(E_F + E_V\right), \quad (1)$$

where $E_{\text{tot}}[D^q]$ is the calculated total energy of a supercell containing the defect D in charge state q. $E_{\text{tot}}[TiO_2, \text{bulk}]$ is the energy of the defect-free supercell. Δn_X is the number of atom specie X being remove (positive) or add (negative) to the supercell to create the defect cell. μ_X is the chemical potential of atoms specie X. E_F and E_V are the electron Fermi energy and the position of the valence band maximum, respectively. To remedy the band gap problems (for LDA calculations), the valence band maximum at the special k points is averaged for E_V.

During the equilibrium growth, if any chemical potential rises above its natural phase value (for e.g., Ti metal, O_2 gas, V metal), then the natural phase would form as an inclusion. These set the upper limit of the possible chemical potential for each element. In order for TiO_2, to grow in equilibrium, it is also required that

$$\mu_{\text{TiO}_2} = \mu_{\text{Ti}} + 2\mu_{\text{o}}, \quad (2)$$

where μ_{TiO_2} is the heat of formation of a molecular formula of TiO_2 (−10.10 eV, calculated value). All chemical potentials are referenced to their natural phases. Additional limitations on the chemical potentials are imposed by the formation of alternative phases containing Ti and O such as TiO (see Ref. [41]).

3. Redox potentials on the TiO_2 surface

While narrowing the band gap of TiO_2 improves its absorption of the sunlight, the redox potential is reduced which is undesirable. The reduced redox potential increases the recombination rate of the (photo excited) carriers; lessening the production of the reactive oxygen species (ROS) that can degrade microorganisms and organic pollutants. Thus it is important to carefully balance the reduction of the band gap and the weakening of the redox potential, in order to achieve the best photocatalytic activity. In our approach, this issue is translated into the choice of suitable co-dopants for a given application. To facilitate the design of impurity energy levels and doping mechanism of co-dopants, we need to examine in detail a set of doping elements and their desired lattice locations.

The photo-induced electron and hole transfer depends on the semiconductor-interface reaction of reactive oxygen species (ROS) as well as their redox potentials on TiO_2 surface as discussed below. Fig. 1 illustrates the redox potentials of major species for photocatalyst disinfection and degradation of organic pollutants compared to those for water splitting. The values of the redox potentials shown in Fig. 1 are shown relative to the potential of the standard hydrogen electrode (SHE) at pH = 7 (see Ref. [50]). The higher negative potential provides higher reducing power whereas the higher positive potential provides higher oxidizing power. In other words, the

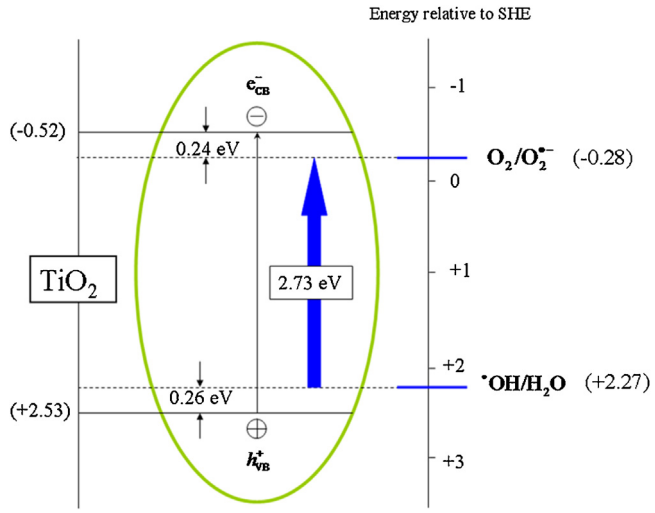

Fig. 1. Potential of the band edges of TiO_2 relatives to major species ($^{\bullet}OH$, $O_2^{\bullet-}$) for photocatalytic degradation for antibacterial agents and organic water pollutants occurring at anatase-TiO_2 surface at pH = 7 [50].

higher the conduction band minimum (CBM) energy, the stronger the reducing power, whereas the lower the valence band maximum (VBM) energy, the higher the oxidizing power. Therefore, the high positive potential and high negative potential of oxidizing species are preferred. On the other hand, to improve the solar absorption, it is necessary to lower the band gap of TiO_2 which would weaken the redox potential of hole and/or electron in the bulk.

To maintain the reaction, the redox potentials should not be weaker than that of the surface-reaction potentials, as illustrated in Fig. 1. The defect levels, which will define the new band edges, should be induced in the energy range between the band edges and the desired reactions. As shown in Fig. 1, the hole potential is +2.53 eV and the electron potential is −0.52 eV with respect to SHE [50]. This indicates that the holes in this system have a very high oxidizing power, whereas the electrons have a much lower reducing power. It reacts with hydroxyl ion OH^- or water H_2O, depending on the pH, on the TiO_2 surface; resulting in hydroxyl radical $^{\bullet}OH$ (+2.27 eV) as a product. An oxygen molecule, O_2, is the main electron scavenger to prevent the electron-hole recombination. O_2 traps photoelectron and turns into superoxide anion $O_2^{\bullet-}$ (−0.28 eV). Both $^{\bullet}OH$ and $O_2^{\bullet-}$ play important roles in the photocatalytic reaction mechanism. To maintain the creation of $^{\bullet}OH$ and $O_2^{\bullet-}$, the new band edge levels should be created within the narrow ranges of 0.26 eV above the VBM and 0.24 eV below the CBM, respectively. Otherwise, the desired surface reactions would be suppressed. The suitable codopants for this work should give defect levels at about 0.24 eV above the VBM and below the CBM which would lead to the total band-gap reduction of about 0.50 eV. The targeted band gap of 2.70 eV would allow significant improvement in generating photoelectrons and photoholes under the solar spectrum.

Recently Gai et al. [3] suggested that the suitable co-dopants in TiO_2 should significantly shift the valence band edge and leave the conduction band edge almost unchanged so that the TiO_2 modified by co-dopants can become an optimized photocatalyst for water splitting applications. This suggestion by Gai et al. is consistent with adjusting the redox potentials for water splitting [3,50]. For water-splitting application TiO_2 is doped with an anion that can induce the energy levels within 1.6 eV above the VBM, while leaving the CBM unchanged. There are various anions that can induce energy levels within this wide energy range. However, the choice of both anion and cation for antibacterial agent application are more stringent. To produce $^{\bullet}OH$ and $O_2^{\bullet-}$, shallow states within 0.26 and 0.24 eV from the VBM and the CBM are required. Any level higher than 0.26 eV above the VBM edge would suppress the $^{\bullet}OH$ production, while any level deeper than 0.24 eV below the CBM edge would suppress the $O_2^{\bullet-}$ production. In addition, the deeper levels that are not fully occupied (or levels that have been charged by photo-excitation) may act as recombination centers that further decrease the photocatalytic activity. Clearly, the criteria for selecting appropriate dopants for antibacterial agent applications are quite different than those for water-splitting.

4. Monodoping in TiO_2

As the first step toward the exploration of the co-doping candidates, we separately substitute both O and Ti sites by a single dopant, i.e., mono-doping. We try to identify potential elements which provide defect energy levels at the desired energy range as described in Fig. 1. Although the energy levels obtained in the single element substitution are expected to be shifted after co-doping due to the pair interactions, these results are still useful as the first approximation on where the levels should lie.

The total density-of-states (DOS) and projected density-of-states (pDOS) of bulk-TiO_2 are consistent with the literature [3]. The valence bands consist mainly of O 2*p* states and the conduction bands show a predominant Ti 3*d* character. Thus it is expected that the replacement of O and Ti by other elements should directly affect the valence bands and conduction bands, respectively. For example, the substitution of Ti by group-III (Sc_{Ti}, Y_{Ti}, Al_{Ti}, Ga_{Ti}, In_{Ti}, and Tl_{Ti}), group-V (V_{Ti}, Nb_{Ti}, Ta_{Ti}, P_{Ti}, As_{Ti}, and Sb_{Ti}), and group-VI (S_{Ti}, Se_{Ti}, Te_{Ti}, Cr_{Ti}, Mo_{Ti}, and W_{Ti},) elements are expected to modify the conduction band edges. And the substitution of O by C, N, and F (i.e., C_O, N_O, and F_O) are expected to modify the valence band edges. In reality, we found that some of the mentioned substitution defects do not lead to any defect levels in the band gap. In Fig. 2, the calculated DOS of selected representatives from each group of dopants are shown to demonstrate the trend of the defect level positions.

For cation doping, Fig. 2(a)–(f) shows the calculated DOS of Ga, Sc, V, Nb, Mo, and Se substituting for Ti (Ga_{Ti}, Sc_{Ti}, V_{Ti}, Nb_{Ti}, Mo_{Ti}, and Se_{Ti}). We found that only V, Mo, and Se induce defect states below the CBM. For anion doping, Fig. 2(g)–(i) shows the calculated DOS of C, N, and F substituting for O (C_O, N_O, and F_O). We found that they induce defect states above the VBM.

As can be seen from Fig. 2(c), (e), and (f), V_{Ti}, Mo_{Ti} and Se_{Ti} have the calculated defect states at 0.55, 0.42, and 0.46 eV below the CBM, respectively. These states are deeper than the desired value of 0.24 eV. Detailed analysis of these defect states reveals that they composed of three defect levels, derived from t_{2g} states of V, Mo and Se 3*d* orbitals. Note that Cr (group-VI element) can also induce defect state in the band gap, however, it is even deeper (not shown in the plot).

For anion doping, only C_O and N_O have defect levels in the band gap, as shown in Fig. 2(g) and (h). F_O does not induce any defect level in the band gap [see Fig. 2(i)]. The C_O defect states, derived from the C 2*p*, are deep and split into three at 0.87, 1.36, and 1.50 eV due to the reduced local symmetry from the lattice distortion around the C atom. For the case of N_O, similar to the case of C_O, there are three defect states above VBM derived from N 2*p*, as shown in Fig. 3(h). Although the defect levels of N_O are shallower (located at 0.47 above the VBM) than those of C_O, they are still deeper than the desired value of 0.26 eV. This partly explains why N-doped TiO_2 has worse photocatalytic activity than that of pure-TiO_2 [51].

Although, none of the studied mono-dopants provides defect levels at the desired positions, the levels may shift toward the desired position when they form co-dopant complexes. For example, N_O by itself may not be a good choice for the enhancement of the photocatalytic activity of TiO_2, but its levels could potentially

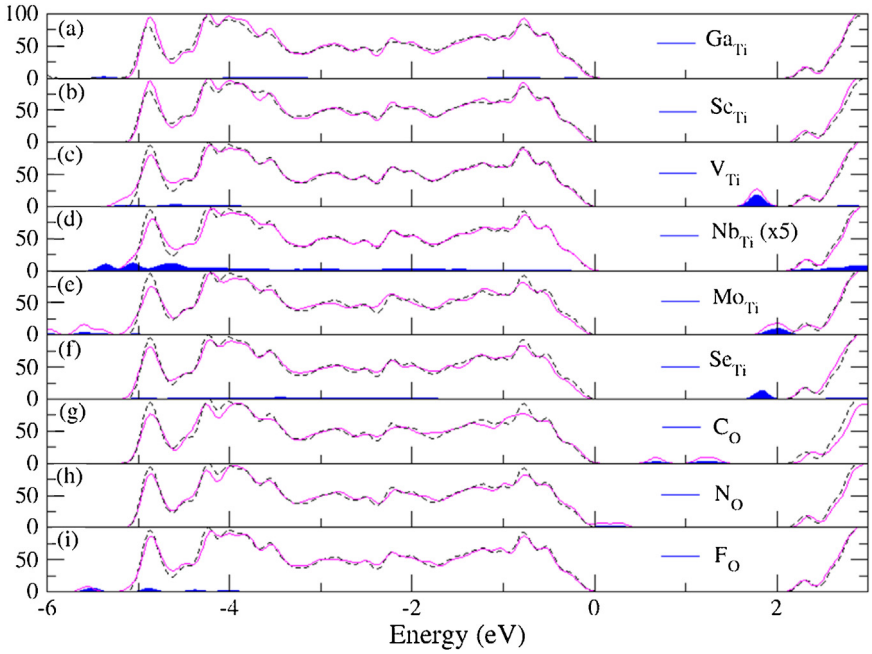

Fig. 2. Site decomposed electron density of states (DOS) by LDA for mono-doping TiO_2 (solid magenta curve) compared with bulk-TiO_2 (dashed black curve). The shaded area refers the PDOS for impurity atoms and is scaled up by a factor given in parentheses for clarity.

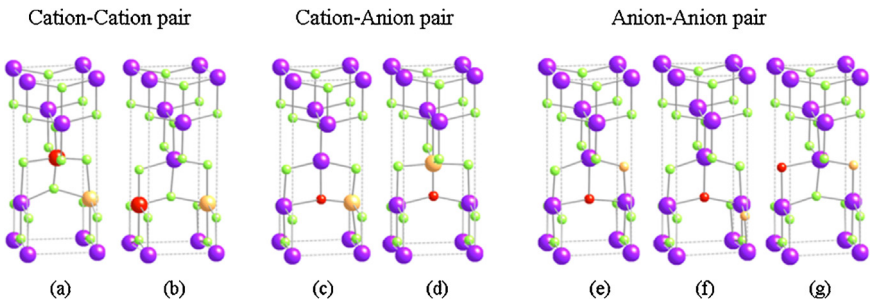

Fig. 3. Schematic illustration of the doping pair configurations for co-doping in TiO_2: (a) and (b) cation–cation pairs, (c) and (d) cation-anion pairs, and (e)–(g) anion–anion pairs. Large purple and small green spheres indicate Ti and O atoms, respectively. Orange and red spheres indicate the sites for replacing the host atoms with the co-doping pairs. (For interpretation of the references to colour in this figure legend, the reader is referred to the web version of this article.)

be reduced down to the desired value by co-doping. Therefore, they are not ruled out from the list of possible co-dopant candidates.

5. Passivated co-doping in TiO_2

To adjust the bandgap to the 'optimum' range for the redox potential without creating the recombination centers, one can utilize the idea of charge-compensated donor-acceptor pairs to preserve the electron counting. For examples, one can co-dope N_O, a single acceptor, with a group-V element such as V_{Ti} or Nb_{Ti}, which is a single donor. In principle, a compensated donor-acceptor pairs can be the pairs of the doping on cation-cation, cation-anion, or anion-anion. Although codoping by substituting cations and anions (i.e., cation-anion pairs) allows the donor-acceptor pairs to form with the minimum separation (hence, gaining the largest Coulombic attraction), in practice, it could be difficult to find the growth conditions that simultaneously favor both cation and anion substitutions. Therefore, codopings purely on the cation site (i.e., cation-cation) or anion site (i.e., anion-anion), despite a larger separation of the pair, could be beneficial for the ease of doping process. Although these types of codopings are likely to give weak interactions between the donor and acceptor, they are worth investigation.

5.1. Searching substitution sites and defect locations

The codoping pairs can be grouped into three types based on the doping sites, i.e., the cation–cation (D_{Ti}-A_{Ti}) pair, cation-anion (D_{Ti}-A_O) pair, and anion–anion (D_O-A_O) pair, as illustrated schematically in Fig. 3. For cation–cation pairs, one can co-dope group-V element, substituting the Ti site, a single donor, with a group-III element substituting the Ti site, a single acceptor. Therefore, we chose the cation–cation pairs of (V_{Ti}-Sc_{Ti}), (V_{Ti}-Y_{Ti}), (V_{Ti}-Ga_{Ti}), (V_{Ti}-In_{Ti}), and (V_{Ti}-Tl_{Ti}). For cation-anion pairs, there are two possible anion elements C_O and N_O, which have comparable size with O atom. For C_O co-dopants, one can co-dope it with group-VI elements substituting the Ti site acting as a double donor (C_O is a double acceptor). The possible C_O co-dopants are (S_{Ti}-C_O), (Se_{Ti}-C_O), (Te_{Ti}-C_O), (S_{Ti}-C_O), and (Mo_{Ti}-C_O). For N_O co-dopants, N_O, a single acceptor, can be co-doped with group-V element substituting the Ti site, which is a single donor. The N_O co-dopants are (V_{Ti}-N_O), (Nb_{Ti}-N_O), (Ta_{Ti}-N_O), (P_{Ti}-N_O), and (As_{Ti}-N_O). For anion–anion pair, the only plausible pair is (F_O-N_O). Other elements of group-VII and -V elements are not suitable due to their large size mismatched with the O site.

Because of the crystal symmetry, each pair type has more than one inequivalent pair configurations. For the case of cation–cation codopant and cation-anion codopant pairs, there are two inequiv-

alent configurations for each, see Fig. 3(a)-(b) and (c)-(d), respectively. For the case of anion–anion pair, there are three inequivalent configurations as shown in Fig. 3(e)–(g). For any given donor-acceptor pair, the pair configurations that allows the donor-acceptor pair to form at the closest proximity always have the lowest energy. The only exception observed is the case of (N_O-F_O) pair. While the expected role of the group-VII F when substitution for group-VI O is a donor, the electronegativity of F is actually so strong such that it behaves as an acceptor. Therefore, the N_O-F_O complex is actually an acceptor–acceptor pair, leading to a repulsion force between N and F instead of an attractive force.

5.2. Density of states and defect levels

The total density of states (DOS) and partial DOS (decomposed by projecting the DOS on the atoms of interest) of studied codoping pairs were calculated. Although we have investigated a total of sixteen codoping pairs, we show in Fig. 4 only the representative cation-anion pairs, namely, (V_{Ti}-N_O) and (Nb_{Ti}-N_O) for N_O co-dopants; (Se_{Ti}-C_O) and (Mo_{Ti}-C_O) for C_O co-dopants; (V_{Ti}-Sc_{Ti}) and (V_{Ti}-Ga_{Ti}) for cation–cation co-dopants, and (F_O-N_O) for anion–anion co-dopant. Other codopant pairs (not shown) are either having unfavorable characteristics or not resulting in any defect state in the band gap.

For the cases of N_O co-dopants, as shown in Fig. 4(a) and (b), the defect states associated with N_O (orange shaded area) are slightly shifted toward the VBM compared to case of mono-doping N_O, resulting in the defect states at 0.22 and 0.39 eV for the (V_{Ti}-N_O) and (Nb_{Ti}-N_O) pairs, respectively. For (V_{Ti}-N_O), the states associated with V_{Ti} also shifted toward the CBM compared to the case of mono-doping V_{Ti}; resulting in the defect states at 0.12 eV (blue shaded area). The shifts of the N_O levels toward the VBM and V_{Ti} levels toward the CBM when compared to their respective mono-doping cases, is consistent with the donor-acceptor level repulsion effects when a donor and an acceptor form a complex pair. For C_O co-dopants, the C states induced by C_O in the (Se_{Ti}-C_O) and (Mo_{Ti}-C_O) are still too deep and not suitable for our application, as shown in Fig. 4(c) and (d). For cation–cation co-dopants, both of (V_{Ti}-Sc_{Ti}) and (V_{Ti}-Ga_{Ti}) have deep states, shown as blue shaded area in Fig. 4(e) and (f), below the CBM in almost the same place as the case of mono-doping V_{Ti}. This is because the interaction between the donor and the acceptor is weak in this case due to a large site separation. As expected, there is no defect level near the VBM because there is no doping on the anion site for these cases. For anion–anion codopant (F_O-N_O), the states associated with N_O shifts toward the VBM; leading to shallow defect levels above the VBM, as shown in Fig. 4(g). Therefore, this co-dopant should increase the photocatalytic activity. This is consistent with experimental observation that (F_O-N_O) can enhance the photocatalytic activity [52].

From the DOS, we can see that (V_{Ti}-N_O) is the only defect pair (among the 16 pairs studied) that introduces the states in the vicinity of the desired positions for antibacterial agent application, i.e., 0.26 and 0.24 eV from the VBM and the CBM. As can be seen in Fig. 4(a), (V_{Ti}-N_O) has the calculated states at 0.12 eV below the CBM and 0.33 eV above the VBM. Therefore, it is a potential candidate for our proposed application. This is consistent with previous theoretical studies [6,40,53]. Although there are theoretical and experimental studies claiming that vanadium-nitrogen (V-N) can increase vis-photocatalytic activity of TiO_2 [6,40], no clear physical explanation has been offered. Here, for the first time, we pointed out the relationship between the redox potentials of $^{\bullet}OH$ and $O_2^{\bullet-}$ and the potentials of photo-holes and photo-electrons of (V_{Ti}-N_O), respectively. Because the calculated donor and acceptor levels of (V_{Ti}-N_O) redefine the band edges of TiO_2 that meet the stringent requirement, the (V_{Ti}-N_O) pair is proposed to be the suitable codopant for antibacterial agent and for the degradation of organic pollutants.

Since LDA is known to give an underestimated band gap, to ensure that the relative positions of the defect levels (with respect to the band edges) obtained from LDA are reliable, the calculations of mono-doping V_{Ti} and N_O as well as the (V_{Ti}-N_O) pair were repeated but using HSE06 exchange correlation. The DOS calculated by using HSE06 are shown in Fig. 5. For V_{Ti}, as shown in Fig. 5(a), there are three defect levels derived from V 3*d* located below the CBM [Fig. 5(a)]. This is similar to the DOS observed in the LDA calculations except the level obtained here is slightly deeper. For N_O, as shown in Fig. 5(b), there are three defect levels derived from N 2*p* located above the VBM composing of a shallow level and two deeper

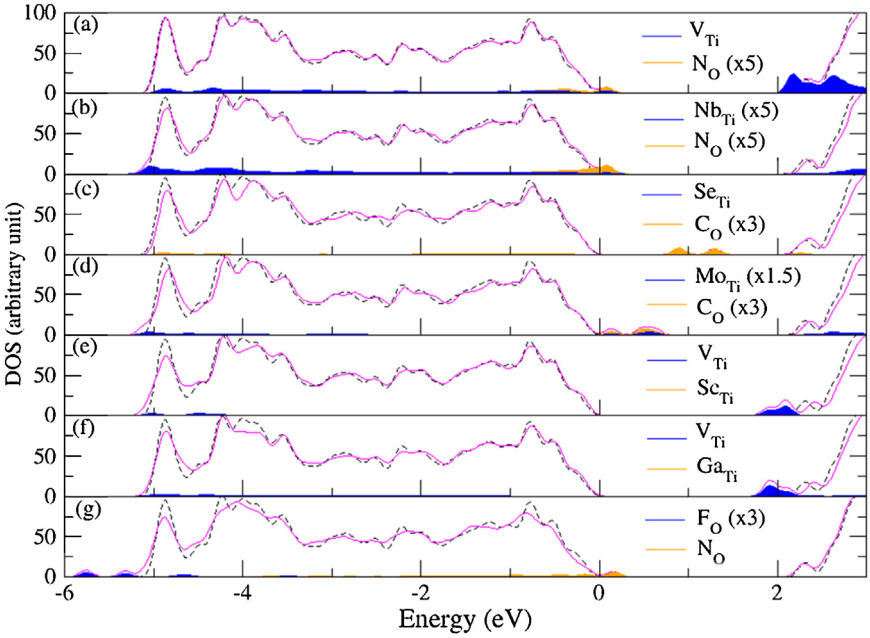

Fig. 4. Site decomposed electron DOS by LDA for codoped TiO_2 (solid magenta curve) compared with that of bulk-TiO_2 (dashed black curve). The filled curves show the PDOS for impurity atoms and are scaled up by a factor given in the parentheses for clarity.

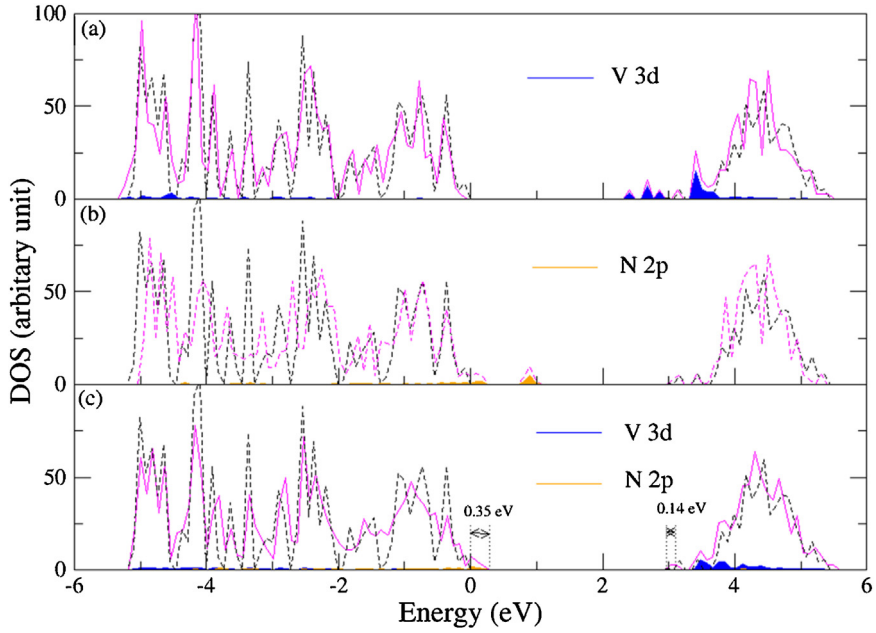

Fig. 5. Site decomposed electron DOS by HSE06 of (a) V_{Ti}, (b) N_O, and (c) V_{Ti}-N_O in TiO_2 (solid magenta curves), compared with that of undoped TiO_2 (dashed black curves). The filled curves show the PDOS for impurity atoms (blue: V 3*d* and green: O 2*p*).

levels. Again, these levels are similar to those obtained from the LDA calculations except they are deeper. For (V_{Ti}-N_O), the defect levels derived from V_{Ti} and N_O are both becomes shallower than those of the isolated defects. Interestingly, the shallowness of the levels of (V_{Ti}-N_O) are agreed with the LDA results to about 15% (with the HSE06 results consistently deeper) despite the fact that the HSE06 results of the mono-doping case give the results deeper by about 50% compared to the LDA results. The values of the defect levels calculated by LDA and HSE06 are compared in Table 1.

From our calculations, the vanadium and nitrogen (V-N) pair is proposed as a suitable cation-anion co-dopant in TiO_2 for an efficient antibacterial agent application because the TiO_2 doped with V-N co-dopant has a reduced band gap that matches the redox potential for of hydroxyl radical (•OH) and superoxide anion ($O_2^{\bullet -}$). Our results are in good agreement with previous experimental studies showing that the V-N codoped TiO_2 photocatalysts show enhanced photocatalytic activity under visible light for the degradation of some organic pollutants such as methylene blue [54–56], pentachlorophenol and its salts [57], rhodamine B [58], 4-chlorophenol [56], and 4-nitrophenol [56]. Most of the previous theoretical studies based on DFT (without the HSE calculations) showed that (V-N) codoped TiO_2 can reduce the bandgap of TiO_2 and should enhance the photocatalytic activity under the visible range of the solar spectrum [40,53,56,59,60]. However, a theoretical study based on TB-LMTO approach proposed that the doping with nitrogen and vanadium should raise the photocatalytic activity of anatase in the nearest UV region [61] instead of in visible region as proposed in present study and other previous studies [40,53,56,59,60]. This discrepancy may rise from the different computational theory used.

For F-N co-doped in TiO_2, we found that the bandgap of TiO_2 is narrowed by the presence of N 2*p* states above the VBM, while the F 2*p* induces defect states below the VBM and do not respond for the bandgap reduction. Our calculated results are in good agreement with previous theoretical study base on DFT [62]. Due to the bandgap reduction, we proposed that the F-N co-doped in TiO_2 can enhance the visible light photocatalytic activities. Experimental results on F-N codoped TiO_2 showed strong visible-light absorption and high photocatalytic activity for *p*-chlorophenol [63], rhodamine B [63], acetaldehyde [64], trichloroethylene [64], and toluene [64] under visible light irradiation. This is consistent with our calculations.

Table 1
The calculated ΔE_v, ΔE_c, and ΔE_g, for anatase-TiO_2 doped with N_O, V_{Ti}, and (V_{Ti}-N_O). Positive values of ΔE_v, ΔE_c, and ΔE_g indicate an increase in energy with respect to undoped-TiO_2 and vice versa. Number in the parentheses are taken from Ref. [40]. Note that the numbers in the table are given in eV.

Impurity	ΔE_v		ΔE_c		ΔE_g	
	HSE	LDA	HSE	LDA	HSE	LDA
V_{Ti}	−0.01	−0.04	−0.80	−0.55	−0.79	−0.51 (−0.52)
N_O	0.66	0.47	0.02	0.04	−0.64	−0.43 (−0.35)
(V_{Ti}-N_O)	0.35	0.33 (0.38)	−0.14	−0.12 (−0.11)	−0.49	−0.45 (−0.49)

Based on our calculated results, both Nb-N and Ta-N co-doped TiO_2 show a similar trend. After doping the band gap of TiO_2 is slightly reduced by the presence of N 2*p* states above the VBM. However, Nb and Ta do not contribute to the bandgap reduction. Our calculated results agree with previous DFT study showing that the bandgap of TiO_2 is slightly narrowed due to the N 2*p* states [65]. There are several experimental studies showing that the photocatalytic oxidation activity evaluated by the decompositions of methylene blue [66] and ethanol [67] were enhanced by the Nb-N co-doping under visible light. For Ta-N, the photocatalytic oxidation activity evaluated by the decompositions of oleic acid, SCN-, Br-, I- [68], ethanol [67] were enhanced by the Ta-N co-doping under visible light, when compared to N single doping. To the best of our knowledge, there is no report on the experimental study of (Nb-N), (Ta-N), (V-N), and (F-N) codoped TiO_2 for antibacterial agent applications.

5.3. Binding energy

To determine the stability of an impurity complex such as (V_{Ti}-N_O) pair, one can calculate the binding energy of a complex [69] defined as

$$E^b = E^f(A) + E^f(B) - E^f(AB), \quad (3)$$

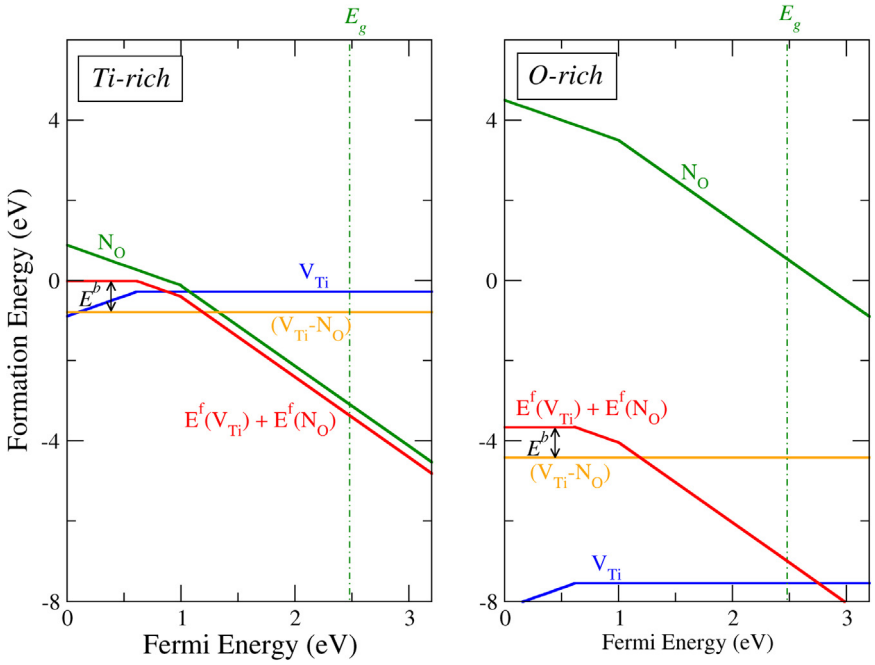

Fig. 6. Formation energies and binding energies of V_{Ti}, N_O, $(V_{Ti}\text{-}N_O)$ codopants, and its isolated form in TiO_2 as a function of the Fermi level, under the Ti-rich (left panel) and O-rich conditions (right Panel), respectively. The slope of the line is an indication of the charge state of the defect. The Fermi energy, referenced to the top of the valence band, is all the way to the experimental band gap. The vertical dotted line is the calculated LDA band gap.

where $E^f(A)$, $E^f(B)$, and $E^f(AB)$ are the formation energies of defects A, B, and a complex defect AB, respectively. A positive binding energy indicates that the complex is bound. The calculated binding energy for $(V_{Ti}\text{-}N_O)$ is 0.77 eV (assuming the electron Fermi energy at the VBM). The strong binding energy of $(V_{Ti}\text{-}N_O)$, indicates that the pair is bound rather strongly and likely to form.

In the process of calculating the binding energy, it is necessary to calculate the formation energy of individual defects as well as the pair. The calculated formation energies of V_{Ti} and N_O, and $(V_{Ti}\text{-}N_O)$ pair are shown in Fig. 6. Our values are in a reasonable agreement with those reported by Ma et al. [40]. Fig. 6 shows the formation energies under two extreme growth conditions, i.e., Ti-rich and O-rich. The binding energy, which is the difference between the sum of the energy of the two parent defects (red line) and the energy of the complex pair (orange line), remains the same for both growth conditions. The binding energy is the highest at 0.79 eV for $E_F < 0.61$ eV. At higher E_F the binding energy is quickly reduced and diminished at $E_F = 1.19$ eV. Note, however, that the formation energy of each individual defect as well as the complex pair can vary depending on the growth condition. Based on our results, the Ti-rich condition can provide all defects with reasonable energy to form and the O-rich condition promotes the formation of V_{Ti} but suppresses the formation of N_O. This plot can serve as a guide to help designing experimental doping conditions to balance the creation of both individual defects to form the pair. For example, one would shift toward the O-rich side to suppress N_O formation and enhance V_{Ti} formation or one could shift the growth condition toward the Ti-rich side to suppress V_{Ti} formation and enhance N_O formation.

6. Conclusions

To aid the quest for the appropriate passivated co-dopants in TiO_2 for the efficient photocatalytic application, we performed comprehensive and systematic first-principles calculations of isolated impurities and impurity pairs in anatase-TiO_2. Based on the redox potential investigation, we proposed that to improve the solar absorption of TiO_2 and preserving high photocatalytic activity for antibacterial purposes, the co-dopant pair should lower the CBM and lift the VBM by about 0.24 eV and 0.26 eV, respectively. Among sixteen pairs studied, we identify that $(V_{Ti}\text{-}N_O)$ is the best candidate that gives the acceptor and donor levels close to the targeted redox potentials for the antibacterial agent and disinfection applications.

The $(V_{Ti}\text{-}N_O)$ pair defect can narrow the bandgap of anatase-TiO_2 while preserving high photocatalytic activity for antibacterial purposes. The complex pair provides the acceptor level about 0.33 eV above the VBM and the donor level at about 0.12 eV below the CBM. This results in the band gap reduction of about 0.45 eV, which would significantly improve the solar photocatalytic activity. The $(V_{Ti}\text{-}N_O)$ pair has a reasonably large binding energy at 0.77 eV; making the pair rather stable against separation. Because LDA calculations underestimate the band gaps, to ensure the reliability of our results, the calculations of $(V_{Ti}\text{-}N_O)$ complex pair were repeated using the HSE06 which can provide band gaps in good agreement with the experiments. The results obtained from HSE06 calculations are consistent with those obtained using LDA, i.e., the pair has shallow accepter and donor levels at 0.35 and 0.14 eV from the VBM and the CBM edges, respectively. The $(V_{Ti}\text{-}N_O)$ pair should improve the absorption of the visible in the solar spectrum by reducing the band gap by 0.49 eV. TiO_2 doped with $(V_{Ti}\text{-}N_O)$ pair also has the redox and oxidizing potentials of photo-holes and photo-electrons that are strong enough to produce $^{\bullet}OH$ and $O_2^{\bullet -}$, ROSs required as antibacterial agent and degradation of organic pollutants.

Acknowledgements

This work was supported by the National Research Foundation of Korea (NRF) funded by the Ministry of Science, ICT & Future Planning (no. 2013R1A2A2A01067950). One of the authors (SN) acknowledges the support from Faculty of Science at Si Racha grant no. 1/2559. Another author (S.L.) was supported by NANOTEC-SUT Center of Excellence on Advanced Functional Nanomaterials. Part of

the computation was carried out at the Synchrotron Light Research Institute (Public Organization), Thailand.

References

[1] M. Ashokkumar, An overview on semiconductor particulate systems for photoproduction of hydrogen, Int. J. Hydrogen Energy 23 (1998) 427–438.
[2] A. Fujishima, K. Honda, Electrochemical photolysis of water at a semiconductor electrode, Nature 238 (1972) 37–38.
[3] Y. Gai, J. Li, S.S. Li, J.B. Xia, S.-H. Wei, Design of narrow-gap TiO_2: a passivated codoping approach for enhanced photoelectrochemical activity, Phys. Rev. Lett. 102 (2009) 036402.
[4] M. Ni, M.K.H. Leung, D.Y.C. Leung, K. Sumathy, A review and recent developments in photocatalytic water splitting using TiO_2 for hydrogen production, Renew. Sustain. Energy Rev. 11 (2007) 401–425.
[5] F. Han, V.S.R. Kambala, M. Srinivasan, D. Rajarathnam, R. Naidu, Tailored titanium dioxide photocatalysts for the degradation of organic dyes in wastewater treatment: a review, Appl. Catal. A 359 (2009) 25–40.
[6] N. Patel, R. Jaiswal, T. Warang, G. Scarduelli, A. Dashora, B.L. Ahuja, D.C. Kothari, A. Miotello, Efficient photocatalytic degradation of organic water pollutants using V–N-codoped TiO_2 thin films, Appl. Catal. B Environ. 150–151 (2014) 74–81.
[7] A. Fujishima, X. Zhang, D.A. Tryk, Heterogeneous photocatalysis: from water photolysis to applications in environmental cleanup, Int. J. Hydrogen Energy 32 (2007) 2664–2672.
[8] J.A. Byrne, P.A. Fernandez-Ibanez, P.S.M. Dunlop, D.M.A. Alrousan, J.W.J. Hamilton, Photocatalytic enhancement for solar disinfection of water: a review, Int. J. Photoenergy (2011) 1–12.
[9] A. Zaleska, J.W. Sobczak, E. Grabowska, J. Hupka, Preparation and photocatalytic activity of boron-modified TiO_2 under UV and visible light, Appl. Catal. B 78 (2008) 92–100.
[10] C. Di Valentin, G. Pacchioni, A. Selloni, Origin of the different photoactivity of N-doped anatase and rutile TiO_2, Phys. Rev. B 70 (2004) 085116–085119.
[11] R. Asahi, T. Morikawa, Nitrogen complex species and its chemical nature in TiO2 for visible-light sensitized photocatalysis, Chem. Phys. 339 (2007) 57–63.
[12] R. Asahi, T. Morikawa, T. Ohwaki, A. Aoki, Y. Taga, Visible-light photocatalysis in nitrogen-doped titanium oxides, Science 293 (2001) 269.
[13] Z.S. Lin, A. Orlov, R.M. Lambert, M.C. Payne, New insights into the origin of visible light photocatalytic activity of nitrogen-doped and oxygen-deficient anatase TiO_2, J. Phys. Chem. B 109 (2005) 20948–20952.
[14] M.C. Long, W.M. Cai, Z.P. Wang, G.Z. Liu, Correlation of electronic structures and crystal structures with photocatalytic properties of undoped, N-doped and I-doped TiO_2, Chem. Phys. Lett. 420 (2006) 71–76.
[15] M. Sathish, B. Viswanathan, R.P. Viswanath, C.S. Gopinath, Synthesis, characterization, electronic structure, and photocatalytic activity of nitrogen-doped TiO_2 nanocatalyst, Chem. Mater. 17 (2005) 6349–6353.
[16] K.S. Yang, Y. Dai, B.B. Huang, Study of the nitrogen concentration influence on N-doped TiO_2 anatase from first-principles calculations, J. Phys. Chem. C 111 (2007) 12086–12090.
[17] J.W. Zheng, A. Bhattcahrayya, P. Wu, Z. Chen, J. Highfield, Z. Dong, R. Xu, The origin of visible light absorption in chalcogen element (S, Se, and Te)-doped anatase TiO_2 photocatalysts, J. Phys. Chem. C 14 (2010) 7063–7069.
[18] S. Matsushima, K. Takehara, K. Yamane, K. Yamada, H. Nakamura, M. Arai, K. Kobayashi, First-principles energy band calculation for undoped and S-doped TiO_2 with anatase structure, J. Phys. Chem. Solids 68 (2007) 206–210.
[19] K. Nishijima, Y. Fujisawa, N. Murakami, T. Tsubota, T. Ohno, Development of an S-doped titania nanotube (TNT) site-selectively loaded with iron(III) oxide and its photocatalytic activities, Appl. Catal. B 84 (2008) 584–590.
[20] T. Ohno, M. Akiyoshi, T. Umebayashi, K. Asai, T. Mitsui, M. Matsumura, Preparation of S-doped TiO2 photocatalysts and their photocatalytic activities under visible light, Appl. Catal. A 265 (2004) 115–121.
[21] F.H. Tian, C.B. Liu, Effects of surface oxygen vacancies on photophysical and photochemical processes of Zn-doped TiO_2 nanoparticles and their relationships, J. Phys. Chem. B 110 (2006) 17866–17871.
[22] T. Umebayashi, T. Yamaki, H. Itoh, K. Asao, Band gap narrowing of titanium dioxide by sulfur doping, Appl. Phys. Lett. 81 (2002) 454–456.
[23] K.S. Yang, Y. Dai, B.B. Huang, Understanding photocatalytic activity of S- and P-doped TiO_2 under visible light from first-principles, J. Phys. Chem. C 111 (2007) 18985–18994.
[24] A.V. Emeline, G.N. Kuzmin, N. Serpone, Wavelength-dependent photostimulated adsorption of molecular O_2 and H_2 on second generation titania photocatalysts: the case of the visible-light-active N-doped TiO_2 system, Chem. Phys. Lett. 454 (2008) 279–283.
[25] S. Kim, S.-J. Hwang, W. Choi, Visible light active platinum-ion-doped TiO_2 photocatalyst, J. Phys. Chem. B 109 (2005) 24260–24267.
[26] R. Sasikala, V. Sudarsan, C. Sudakar, R. Naik, T. Sakuntala, S.R. Bharadwaj, Enhanced photocatalytic hydrogen evolution over nanometer sized Sn and Eu doped titanium oxide, Int. J. Hydrogen Energy 33 (2008) 4966–4973.
[27] M.K. Seery, R. George, P. Floris, S.C. Phillai, Silver doped titanium dioxide nanomaterials for enhanced visible light photocatalysis, J. Photochem. Photobiol. A 189 (2007) 258–263.
[28] G. Shao, Electronic structures of manganese-doped rutile TiO_2 from first principles, J. Phys. Chem. C 112 (2008) 18677–18685.
[29] A.P. Singh, S. Kumari, R. Shrivastav, S. Dass, V.R. Satsangi, Iron doped nanostructured TiO_2 for photoelectrochemical generation of hydrogen, Int. J. Hydrogen Energy 33 (2008) 5363–5368.
[30] J.M. Herrmann, J. Disdier, P. Pichat, Effect of chromium doping on the electrical and catalytic properties of powder titania under UV and visible illumination, Chem. Phys. Lett. 108 (1984) 618–622.
[31] W. Mu, J.M. Herrmann, P. Pichat, Room temperature photocatalyst oxidation of liquid cyclohexane into cyclohexanone over neat and modified TiO_2, Catal. Lett. 3 (1989) 73–84.
[32] K.-S. Ahn, Y. Yan, S. Shet, T. Deutsch, J. Turner, M. Al-Jassim, Enhanced photoelectrochemical responses of ZnO films through Ga and N codoping, Appl. Phys. Lett. 91 (2007) 231909–231912.
[33] M.N. Huda, Y. Yan, S.-H. Wei, M. Al-Jassim, Electronic structure of ZnO:GaN compounds: asymmetric bandgap engineering, Phys. Rev. B 78 (2008) 195204–195208.
[34] P.E. Blöchl, Projector augmented-wave method, Phys. Rev. B 50 (1994) 17953–17979.
[35] G. Kresse, J. Furthmüller, Efficiency of ab-initio total energy calculations for metals and semiconductors using a plane-wave basis set, Comput. Mater. Sci. 6 (1996) 15–50.
[36] C.J. Howard, T.M. Sabine, F. Dickson, Structural and thermal parameters for rutile and anatase, Acta Crystallogr. Sect. B: Struct. Sci. 47 (1991) 462–468.
[37] R. Asahi, Y. Taga, W. Mannstadt, A.J. Freeman, Electronic and optical properties of anatase TiO_2, Phys. Rev. B 61 (2000) 7459–7465.
[38] M. Calatayud, P. Mori-Sánchez, A. Beltrán, A.M. Pendás, E. Francisco, J. Andrés, J.M. Recio, Quantum-mechanical analysis of the equation of state of anatase TiO_2, Phys. Rev. B 64 (2001) 184113–184121.
[39] A. Fahmi, C. Minot, B. Silvi, M. Causá, Theoretical analysis of the structures of titanium dioxide crystals, Phys. Rev. B 47 (1993) 11717–11724.
[40] X. Ma, L. Miao, S. Bie, J. Jiang, Synergistic effect of V/N-codoped anatase TiO2 photocatalysts, Solid State Commun. 150 (2010) 689–692.
[41] S. Na-Phattalung, M.F. Smith, K. Kim, M.-H. Du, S.-H. Wei, S.B. Zhang, S. Limpijumnong, First-principles study of native defects in anatase TiO_2, Phys. Rev. B 73 (2006) 125205–125210.
[42] H. Tang, H. Berger, P.E. Schmid, F. Lévy, G. Burri, Photoluminescence in TiO_2 anatase single crystals, Solid State Commun. 87 (1993) 847–850.
[43] J. Heyd, G.E. Scuseria, M. Ernzerhof, Hybrid functionals based on a screened Coulomb potential, J. Chem. Phys. 118 (2003) 8207–8215.
[44] J. Heyd, G.E. Scuseria, M. Ernzerhof, Erratum: hybrid functionals based on a screened Coulomb potential, J. Chem. Phys. 124 (2006) 219906.
[45] J. Paier, M. Marsman, K. Hummer, G. Kress, I.C. Gerber, J.G. Angyan, Screened hybrid density functionals applied to solids, J. Chem. Phys. 124 (2006) 154709–154721.
[46] J.E. Northrup, S.B. Zhang, Energetics of the As vacancy in GaAs: the stability of the 3+ charge state, Phys. Rev. B 50 (1994) 4962–4964.
[47] S.B. Zhang, J.E. Northrup, Chemical potential dependence of defect formation energies in GaAs: application to Ga self-diffusion, Phys. Rev. Lett. 67 (1991) 2339–2342.
[48] S.B. Zhang, S.-H. Wei, A. Zunger, Intrinsic *n*-type versus *p*-type doping asymmetry and the defect physics of ZnO, Phys. Rev. B 63 (2001) 075205–075211.
[49] H.J. Monkhorst, J.D. Pack, Special points for Brillouin-zone integrations, Phys. Rev. B 13 (1976) 5188–5192.
[50] A. Fujishima, Titanium dioxide photocatalysis, J. Photochem. Photobiol. C: Photochem. Rev. 1 (2000) 1–21.
[51] K. Hashimoto, H. Irie, A. Fujushima, TiO_2 photocatalysis: a historical overview and future prospects, Jpn. J. Appl. Phys. 44 (Pt 1) (2005) 8269–8285.
[52] Y. Cong, J.L. Zhang, F. Chen, M. Anpo, Synthesis and characterization of nitrogen-doped TiO2 nanophotocatalyst with high visible light activity, J. Phys. Chem. C 111 (2007) 6976–6982.
[53] Z. Zhao, Q. Liu, Designed highly effective photocatalyst of anatase TiO_2 codoped with nitrogen and vanadium under visible-light irradiation using first-principles, Catal. Lett. 124 (2008) 111–117.
[54] D.E. Gu, B.C. Yang, Y.D. Hu, V and N co-doped nanocrystal anatase TiO2 photocatalysts with enhanced photocatalytic activity under visible light irradiation, Catal. Commun. 9 (2008) 1472–1476.
[55] N.H. Ke, P.N.T. Hang, L.V.T. Hung, Investigating the photocatalytic activity under visible region of nitrogen and vanadium Co-dopped TiO2 thin film prepared by DC reactive magnetron Co-sputtering method, Int. J. Energy Trends Eng. Appl. Sci. 3 (2012) 45–48.
[56] N. Patel, R. Jaiswal, T. Warang, G. Scarduelli, A. Dashora, B.L. Ahuja, D.C. Kothari, A. Miotello, Efficient photocatalytic degradation of organic water pollutants using V-N-codoped TiO2 thin films, Appl. Catal. B: Environ. 150 (2014) 74–81.
[57] J.W. Liu, R. Han, Y. Zhao, H.T. Wang, W.J. Lu, T.F. Yu, Y.X. Zhang, Enhanced photoactivity of V-N codoped TiO2 derived from a two-step hydrothermal procedure for the degradation of PCP-Na under visible light irradiation, J. Phys. Chem. C 115 (2011) 4507–4515.
[58] R. Jaiswal, N. Patel, D.C. Kothari, A. Miotello, Improved visible light photocatalytic activity of TiO2 co-doped with vanadium and nitrogen, Appl. Catal. B: Environ. 126 (2012) 47–54.
[59] J. Xu, C. Chen, X. Xiao, L. Liao, L. Miao, W. Wu, F. Mei, A.L. Stepanov, G. Cai, Y. Liu, Z. Dai, F. Ren, C. Jiang, J. Liu, Synergistic effect of V/N codoping by ion implantation on the electronic and optical properties of TiO2, J. Appl. Phys. 115 (2014) 143106.

[60] Q. Meng, T. Wang, E. Liu, X. Ma, Q. Geac, J. Gong, New insight into the enhanced visible-light photocatalytic activities of B-, C- and B/C-doped anatase TiO2 by first-principles, Phys. Chem. Chem. Phys. 15 (2013) 9549.
[61] V.P. Zhukov, V.M. Zainullina, The effect of crystal lattice distortions on the electronic band structure and optical properties of the N,V- and N, Na-doped anatase, Phys. B (Amst., Neth.) 406 (2011) 3752–3758.
[62] J. Lu, H. Jin, Y. Dai, K. Yang, B. Huang, Effect of electronegativity and charge balance on the visible-light-responsive photocatalytic activity of nonmetal doped anatase TiO2, Int. J. Photoen. 928503 (2012) 1–8.
[63] D.G. Huang, S.J. Liao, J.M. Liu, Z. Dang, L. Petrik, Preparation of visible-light responsive N-F-codoped TiO2 photocatalyst by a sol-gel-solvothermal method, J. Photochem. Photobiol. A 184 (2006) 282.
[64] D. Li, H. Haneda, S. Hishita, N. Ohashi, Visible-light-driven N-F-Co doped TiO2 photocatalysts. 2. Optical characterization, photocatalysis, and potential application to air purification, Chem. Mater. 17 (2005) 2596.
[65] X. Ma, Y. Wu, Y. Lu, J. Xu, Y. Wang, Y. Zhu, Effect of compensated codoping on the photoelectrochemical properties of anatase TiO2 photocatalyst, J. Phys. Chem. C 115 (2011) 16963–16969.
[66] T.M. Breault, B.M. Barlett, Composition dependence of TiO2:(Nb,N)-x compounds on the rate of photocatalytic methylene blue dye degradation, J. Phys. Chem. C 117 (2013) 8611–8618.
[67] L. Rimoldi, C. Ambrosi, G.D. Liberto, L.L. Presti, M. Ceotto, C. Oliva, D. Meroni, S. Cappelli, G. Cappelletti, G. Soliveri, S. Ardizzone, Impregnation versus bulk synthesis: how the synthetic route affects the photocatalytic efficiency of Nb/Ta:N codoped TiO2 nanomaterials, J. Phys. Chem. C 119 (2015) 24104–24115.
[68] K. Obata, H. Irie, K. Hashimoto, Enhanced photocatalytic activities of Ta, N co-doped TiO2 thin films under visible light, Chem. Phys. 339 (2007) 124.
[69] C.G. Van de Walle, J. Neugebauer, First-principles calculations for defects and impurities: applications to III-nitrides, J. Appl. Phys. 95 (2004) 3851–3879.